Contents lists available at SciVerse ScienceDirect

Journal of Quantitative Spectroscopy & Radiative Transfer

journal homepage: www.elsevier.com/locate/jqsrt

Spectral optical properties of selected photosynthetic microalgae producing biofuels

Euntaek Lee, Ri-Liang Heng, Laurent Pilon*

Mechanical and Aerospace Engineering Department, Henry Samueli School of Engineering and Applied Science, University of California, 420 Westwood Plaza, Eng. IV 37-132, Los Angeles, CA 90095, USA

ARTICLE INFO

ABSTRACT

This paper presents the spectral complex index of refraction of biofuel producing photosynthetic microalgae between 400 and 750 nm. They were retrieved from their experimentally measured average absorption and scattering cross-sections. The microalgae were treated as homogeneous polydisperse spheres with equivalent diameter such that their surface area was identical to that of their actual spheroidal shape. An inverse method was developed combining Lorentz–Mie theory as the forward method and genetic algorithm. The unicellular green algae *Chlamydomonas reinhardtii* strain CC125 and its truncated chlorophyll antenna transformants *tla1*, *tlaX*, and *tla1-CW+* as well as *Botryococcus braunii*, *Chlorella sp.*, and *Chlorococcum littorale* were investigated. These species were selected for their ability to produce either hydrogen gas or lipids for liquid fuel production. Their retrieved real and imaginary parts of the complex index of refraction were continuous functions of wavelength with absorption peaks corresponding to those of *in vivo* Chlorophylls *a* and *b*. The T-matrix method was also found to accurately predict the experimental measurements by treating the microalgae as axisymmetric spheroids with the experimentally measured major and minor diameter distributions and the retrieved spectral complex index of refraction. Finally, pigment mass fractions were also estimated from the retrieved absorption index. The method and/or the reported optical properties can be used in various applications from ocean remote sensing, carbon cycle study, as well as photobiological carbon dioxide mitigation and biofuel production.

1. Introduction

Photobiological carbon dioxide (CO_2) fixation and biofuel production have received major academic and industrial interest in recent years due to rising concerns over global warming, fossil fuel cost, as well as energy security. The technology consists of providing CO_2 and sunlight to selected species of microorganisms grown in photobioreactors. These microorganisms, in turn, grow and may produce (i) gases such as methane and hydrogen or (ii) lipids which can be converted to liquid fuels, depending on the species and growth conditions.

Solar radiation is the energy source driving the metabolic activity of photosynthetic microorganisms. As light penetrates into the photobioreactor, it is absorbed and scattered by the microorganisms. Light transfer in photobioreactors is governed by the radiative transfer equation (RTE). The latter is an energy balance on the radiative energy traveling along a particular direction ŝ. The absorption and scattering coefficients of microalgae along with the scattering phase function are major parameters needed to solve the RTE for simulating, designing, scaling-up, optimizing, and controlling photobioreactors [1].

* Corresponding author. Tel.: +1 310 206 5598;
fax: +1 310 206 2302.
E-mail address: pilon@seas.ucla.edu (L. Pilon).

These characteristics are strongly dependent on wavelength and vary from one species to another. They can be determined either experimentally [2,3] or based on electromagnetic wave theory [4]. This latter approach often assumes that the scatterers have relatively simple shape (e.g., spherical) and ignore their heterogeneous nature by attributing them a uniform effective complex index of refraction [5,6]. Pottier et al. [4] recognized that for complex microorganisms shapes (e.g., cylinders and spheroids), advanced numerical tools are required to predict their absorption and scattering coefficients and scattering phase function collectively called radiation characteristics. On the other hand, experimental measurements account for the actual shape, morphology, and size distribution of the microorganisms. However, experimental setups can be expensive and measurements are time consuming.

In order to design, optimize, and operate photobioreactors for CO_2 fixation and biofuel production, it would be convenient to have the ability to predict the radiation characteristics of microalgae from first principles instead of carrying out costly and time consuming experiments. If the effective spectral real and imaginary parts of the complex index of refraction as well as the microorganisms shape and size distribution are known to within an acceptable level of uncertainties, the absorption and scattering coefficients can be predicted by Lorentz–Mie theory [7], if the microalgae are spherical, or by the T-matrix method [8], if the particles have more complex shapes.

The present study aims to retrieve the spectral real part (or refraction index) and imaginary part (absorption index) of the complex index of refraction of microalgae from experimentally measured size distribution as well as absorption and scattering cross-sections [3,9]. The green algae *Chlamydomonas reinhardtii* strain CC125 and its truncated chlorophyll antenna transformants *tla1*, *tlaX*, and *tla1-CW*$^+$ [3] as well as *Botryococcus braunii*, *Chlorella sp.*, and *Chlorococcum littorale* [9] were considered in this study. Finally, the results were used to retrieve the microalgae pigment concentrations and gain insight into their composition.

2. Background

2.1. Microbial light harvesting pigments

Photosynthesis begins with the absorption of photons by the photosynthetic apparatus which consists of three major components (i) the reaction center, (ii) the core antenna, and (iii) the peripheral antenna. Photochemical charge separation and electron transport take place in the reaction center [10]. The core antenna contains the photosynthetic pigments chlorophylls or bacteriochlorophylls. It is surrounded by the peripheral antenna which is an assembly of chlorophylls, bacteriochlorophylls, and other accessory pigments such as carotenoids and phycobiliproteins. The peripheral antenna is particularly important in channeling additional photon energy to the reaction center at small light intensities. In microalgae and
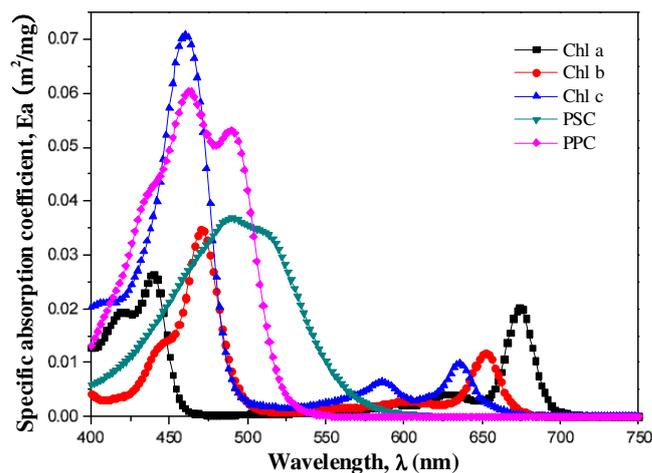

Fig. 1. *In vivo* specific absorption coefficient *Ea* (in m²/mg) of primary pigments chlorophylls *a*, *b*, and *c* and photosynthetic carotenoids (PSC), and photoprotective carotenoids (PPC) over the spectral region from 400 to 750 nm [12].

cyanobacteria, the photosynthetic apparatus is located on the photosynthetic membrane called thylakoid [11].

Different pigment molecules absorb over different spectral bands of the visible and near infrared parts of the spectrum enabling more efficient utilization of solar energy. Fig. 1 shows the *in vivo* specific absorption coefficient *Ea* (in m²/mg) of primary pigments chlorophylls *a*, *b*, and *c* as well as accessory pigments such as photosynthetic carotenoids (PSC), and photoprotective carotenoids (PPC) measured over the spectral region from 400 to 750 nm [12]. It indicates that Chlorophyll *a* (Chl *a*) absorbs around 435 and 676 nm while Chlorophyll *b* (Chl *b*) absorbs around 475 and 650 nm. Since they do not absorb green light ($\lambda \approx 520-570$ nm) significantly, these microalgae appear green to the human eye. On the other hand, carotenoids are accessory pigments found in all photosynthetic microorganisms. They absorb mainly in the blue part of the spectrum (400 nm $\leq \lambda \leq$ 550 nm) [10]. Carotenoids serve two major functions (i) shielding the photosynthetic apparatus from photo-oxidation under large light intensities and (ii) increasing the solar light utilization efficiency by expanding the absorption spectrum of the microorganism.

The intracellular pigments such as chlorophylls and carotenoids are typically extracted by using organic solvents which penetrate through the cell membrane and dissolves the lipids to extract pigments [13,14]. Methanol, acetone, and ethanol are usually used as the organic solvents in the pigments extraction process [15,16]. Overall, measuring the pigment concentration can be very time consuming and suffers from various and sometimes large experimental uncertainties [13].

C. reinhardtii contains Chl *a* and Chl *b* and photoprotective carotenoids (PPC) [4]. Pottier et al. [4] measured their mass fraction by acetone extraction and optical density measurements as 1.4 wt.%, 0.7 wt.%, and 0.45 wt.%, respectively. Berberoğlu et al. [9] measured the mass concentrations (in g/kg of dry weight) of Chl *a* and Chl *b* for microalgae *C. littorale*, *B. braunii*, and *Chlorella sp.* using ethanol extraction method [11]. Unfortunately, their

measurements do not agree with results from other studies reported in the literature and may be erroneous. First, Belcher [17] reported the ratio of concentrations of Chl *a* to Chl *b* in *B. braunii* as 1.35. Similarly, Tanoi et al. [18] reported the mass fraction of Chl *a+b* in *B. braunii* grown under various conditions to be in the range from 0.22 to 0.56 dry wt.%. In addition, Brown [19] reported the mass fraction of Chl *a* and Chl *b* in two strains of *Chlorella sp.* to be in the range from 0.23 to 1.02% and from 0.17 to 0.53%, respectively. The author also found that the concentration of Chl *a* was consistently larger than the concentration of Chl *b* in the ratio 1.35 to 2.6. Finally, Hu et al. [20] measured the Chl *a* and Chl *b* mass fractions of *C. littorale* under optimum growth conditions as 1.4% and 0.5%, respectively. These results were further supported by Schnackenberg et al. [21] who reported the ratio of the concentrations of Chl *a* to Chl *b* in *C. littorale* in the range of 1.52–2.08. Note that the microalgae size, composition, and pigment concentrations vary depending on the growth conditions. These variations along with the spectral resolution of the spectrometer and the choice of correlation between pigment concentration and optical densities may contribute to discrepancies.

2.2. Radiation characteristics of microalgae

A large body of the literature exists on predicting and measuring the absorption and scattering coefficients and the scattering phase function of microalgal suspension [1,5,22–24].

Bidigare et al. [12] used a predictive approach to determine the absorption coefficient in various species of phytoplankton. The cell was modeled as a homogeneous particle in which only the pigments in the cell contributed to the absorption coefficient in the photosynthetically active radiation (PAR) region between 400 and 700 nm. Then, the absorption coefficient (in 1/m) was expressed as [25]

$$\kappa_\lambda = \sum_{i=1}^{N} Ea_i C_i \tag{1}$$

where Ea_i (in m^2/kg) is the *in vivo* specific spectral absorption coefficient of pigment i (Fig. 1) and C_i is its mass concentration (in kg/m^3).

Pottier et al. [4] used a similar approach to predict the spectral absorption coefficient of *C. reinhardtii* by assuming that the pigments were uniformly distributed within the cell and only Chl *a*, Chl *b*, and PPC were present. The authors modified the expression for the absorption coefficient given by Bidigare et al. [12] to express it in terms of pigment mass fractions as

$$\kappa_\lambda = \rho_{dm} \frac{1-x_w}{x_w} \sum_{i=1}^{N} Ea_i w_i \tag{2}$$

where ρ_{dm} is the density of dry material in the biomass (in kg/m^3), x_w is the volume fraction of water in the cell, while w_i is the dry mass fraction of pigment i.

Moreover, Quirantes and Bernard [26] modeled algal cells as two-layer particles with an inner core and an external coating. The coating was assumed to be non-absorbing and had a refraction index of 1.36. The inner core was absorbing and featured a larger refraction index than the outer coating. Its value was selected such that the volume-averaged complex index of refraction of the composite particle was equal to that of an equivalent homogeneous scatterer with complex index of refraction of $1.40 + i0.005$, considered to be typical of microbial cells [6,27,28]. First, the extinction and absorption efficiency factors of homogeneous spheres and coated spheres were calculated using the Aden–Kerker theory [29] and the modified anomalous diffraction approximation (ADA) [30], respectively. The heterogeneous geometry of the coated spheres was found to increase the back-scattering efficiency by a factor as high as 50 but had negligible effects on the absorption efficiency factor and weak effects on the scattering efficiency factor when compared with those of a homogeneous sphere with the same complex index of refraction. These results were consistent with previous studies using volume-averaged equivalent complex indices of refraction to compare homogeneous and heterogeneous multi-layered spheres [31,32]. In addition, Quirantes and Bernard [26] considered three different geometries with the same size parameter and equivalent complex refractive index namely (i) off-centered coated spheres, (ii) concentric spheroids, and (iii) concentric spheres. The T-matrix method [33] was used to compute the efficiency factors of the aspherical and non-concentric composite cells. The absorption and scattering efficiency factors showed little dependency on particle shape.

Mishchenko and Travis [34] concluded that particles that were even moderately aspherical could not be approximated as equivalent spheres of diameter d_s when calculating their scattering efficiency factors for size parameter $\chi = \pi n_2 d_s / \lambda$ less than 5–15 where n_2 is the refraction index of the surrounding medium and λ is the wavelength of the incident radiation in a vacuum. In fact, the scattering cross-section of spheroids computed using the T-matrix method was found to be up to 30% smaller than that of equivalent spheres with the same cross-sectional areas for $\chi \approx 1$. The difference in scattering cross-sections between spheroids and equivalent spheres was found to decrease as the size parameter increases. Note that in the present study, the size parameters χ for the different microalgae were larger than 60. Thus, previous studies confirmed the view that treating microalgae with aspect ratio less than 1.5 as spherical can be applied to infer their optical properties from their measured absorption and scattering coefficients [5,6, 35–37].

Recently, Berberoğlu and co-workers [2,3] experimentally measured the radiation characteristics of several H$_2$ producing microorganisms namely (a) purple non-sulfur bacteria *Rhodobacter sphaeroides* [2], (b) cyanobacteria *A. variabilis* [2], and (c) green algae *Chlamydomonas reinhardtii* strain CC125 and its truncated chlorophyll antenna transformants *tla1*, *tlaX*, and *tla1-CW$^+$* [3]. The authors also measured the radiation characteristics of the lipid producing microalgae *C. littorale*, *B. braunii*, and *Chlorella sp.* [9]. Except for the purple bacteria *R. sphaeroides* which absorbs in the near infrared, the absorption coefficients of these microorganisms vanish beyond 750 nm when only scattering contributes to extinction. For example, the wild

strain *C. reinhardtii* CC125 absorbs mainly in the spectral region from 300 to 700 nm with absorption peaks at 435 and 676 nm corresponding to absorption peaks of *in vivo* chlorophyll *a*. It also has additional absorption peaks at 475 and 650 nm corresponding to absorption by chlorophyll *b*. Berberoğlu et al. [3] also showed that the genetically engineered strains of *C. reinhardtii* have less chlorophyll pigments than the wild strain and thus have smaller absorption cross-sections. In particular, the mutant *tlaX* featured a significant reduction in chlorophyll *b* concentration. For all mutants, the reduction in their absorption cross-section was accompanied by an increase in their scattering cross-section.

2.3. Effective optical properties of microorganisms

2.3.1. Direct experimental measurements

The refraction index n_λ of microalgae can be measured directly [6,38–40]. However, the experimental measurements are complicated by the polydispersion of the microbial particles and by light absorption. On the other hand and to the best of our knowledge, no method has been reported in the literature to directly measure the absorption index k_λ of microbial particles in suspension.

First, photometric immersion refractometry consists of suspending the cells in a medium of known refraction index and measuring the transmittance T_λ or the optical density (OD) of the suspension defined as $OD_\lambda = -\log T_\lambda$ [41,42] at a non-absorbing wavelength. For example an aqueous solution of bovine serum albumin (BSA) can be used as the immersion medium as it is not toxic to microorganisms. Solutions with different refraction indices can be prepared by varying the BSA concentration [43]. The OD of the suspension is then measured as a function of BSA concentration. The refraction index of the microbial cells at the wavelength considered is taken as that of the BSA solution corresponding to the minimum OD.

Flow cytometry can also be used to directly measure the refraction index n_λ of microalgae [39,40]. Collimated laser radiation is directed at a stream of saline solution containing microbial particles. The latter are assumed to be homogeneous spheres despite their potentially irregular morphologies. The intensities of forward scattered light (typically at an angle of 1–19° with respect to the incident beam direction), side scattered light (54–126°), and chlorophyll fluorescence (660–700 nm) are measured [39]. The system is calibrated using standard suspensions consisting of polydisperse spherical particles of known refraction index such as oil globules and glass beads. For every individual cell, different intensities of the forward and side scattered light are measured depending on their size, shape, and refraction index. The refraction index is found by fitting the experimental measurements and comparing with standards suspensions.

Finally, the abundance of refraction index data for various species of phytoplankton has been used to correlate the refraction index n_λ to the intracellular carbon concentration in the form [5]

$$n_\lambda = n_{0,\lambda} + n_{1,\lambda} C_c \qquad (3)$$

where $n_{0,\lambda}$ and $n_{1,\lambda}$ are constants determined by experimental procedures and C_c is the intracellular carbon concentration (in kg/m^3). For example, DuRand and Olson [44] reported $n_{0,\lambda} = 1.02$ and $n_{1,\lambda} = 0.000117$ for *Nannochloris sp.* at 665 nm. Unfortunately, most of the above methods measured the refraction index at a single wavelength. It then has to be assumed constant over the PAR for spectral calculations of light transfer in the suspension and estimation of the average fluence rate available in PBRs and necessary in growth kinetic models [4,5,45,46].

2.3.2. Model-based measurements

Despite their heterogeneous morphologies, microalgae have typically been treated as homogeneous with some effective refraction and absorption indices. Stramski and Mobley [24] experimentally measured the size distributions of various marine microbial particles and their spectral radiation characteristics in the PAR region (400–700 nm). The experimental data were used as input to an inverse method developed by Bricaud and Morel [6] to predict the complex refractive index of the particles under the assumptions that the particles were homogeneous and spherical. First, the absorption index was determined based on the anomalous diffraction approximation describing the absorption coefficient as a monotonic function of the absorption thickness parameter defined as $p' = 4\chi k_\lambda$ [30,47] where k_λ is the absorption index of the particle and $\chi = \pi d_s n_2 / \lambda$ is the size parameter previously defined. For any given wavelength and particle size distribution, the absorption index was uniquely related to the absorption coefficient. Thus, for a given wavelength, the absorption index k_λ was varied iteratively until the calculated absorption coefficient matched its experimental value. Calculations were repeated for each wavelength to obtain the spectral absorption index. On the other hand, the refraction index n_λ was derived through an inverse method described by Stramski et al. [37]. Here, the Lorentz–Mie theory [29] was used instead of the anomalous diffraction approximation. The experimental data and the previously retrieved absorption indices were used as input parameters into the Lorentz–Mie theory code [29]. The refraction index was varied iteratively until the calculated extinction coefficient matched its experimental value. It was found that the measured microbial particles had absorption index ranging between 0 and 0.01 and refraction index between 1.38 and 1.42. The refraction index was found to vary by less than 5% in the PAR region for all microorganism species considered.

Pottier et al. [4] adopted a simpler approach to retrieve the refraction and absorption indices of *C. reinhardtii*. They measured the normal hemispherical transmittance of a suspension of *C. reinhardtii* at 820 nm where they do not absorb. The corresponding refraction index was found to be 1.527 and assumed to be constant over the PAR. Then, the authors estimated the spectral absorption index k_λ according to [4]

$$k_\lambda = \frac{\kappa_\lambda \lambda}{4\pi} = \frac{\lambda}{4\pi} \rho_{dm} \frac{1-x_w}{x_w} \sum_{i=1}^{N} Ea_i w_i \qquad (4)$$

where pigment mass fractions w_i were estimated experimentally.

3. Analysis

3.1. Microorganisms

The different microalgae species investigated were selected for different reasons. First, *C. reinhardtii* is one of the best candidates for photobiological hydrogen production as it can produce only H_2 by reversibly shutting down its O_2 production metabolism by sulphur deprivation [48]. They can also be genetically modified with truncated light harvesting chlorophyll antenna. In fact, Polle et al. [49] genetically engineered *C. reinhardtii* via DNA insertional mutagenesis to obtain the mutant strain *tla1* with permanently reduced number of chlorophyll molecules per photosystem, i.e., truncated light harvesting chlorophyll antenna. This strain did not contain cell wall [49]. However, cell walls protect the cells from excessive shear stress such as that observed in photobioreactors for example [49]. Thus, Polle et al. [49] crossed *tla1* with a cell wall containing strain and isolated the strain *tla1-CW$^+$* showing observable characteristics (phenotype) of *tla1* and having a cell wall. In addition, the strain *tlaX* had even a smaller chlorophyll antenna than *tla1*. Finally, the authors reported that the microorganisms with less pigments had higher quantum yield, photosynthesis rate, and light saturation irradiance [49]. Moreover, *B. braunii* grows in freshwater and was chosen for its high lipid content which can be converted into liquid biofuels [50–53]. On the other hand, *Chlorella sp.* is a unicellular green algae with high oil content and fast growth rate under large CO_2 concentrations [53–55]. Finally, *C. littorale* is also of interest because it is a marine microalgae that can tolerate high CO_2 concentrations and can grow to very large cell density [20,56].

3.2. Assumptions

In the present study, the different microalgae were assumed to be spherical. This assumption simplifies the calculations of their radiation characteristics by using the Lorentz–Mie theory instead of the T-matrix method. It has been validated by Quirantes and Bernard [26] and its validity for the microalgae of interest will be discussed later. Moreover, despite their heterogeneous structure, microalgae were treated as homogeneous with some effective refraction and absorption indices. Note that n_λ was treated as wavelength dependent over the PAR, unlike what previous studies have often assumed [4].

3.3. Equivalent diameter and size distribution

The different microalgae were treated as homogeneous spheres with an equivalent diameter such that their surface area was identical to that of their actual spheroidal shape assumed to be axisymmetric [26,57,58]. The polar radius of an axisymmetric spheroid in the spherical coordinate system is given by [34]

$$r(\theta) = \frac{a}{2}\left(\sin^2\theta + \frac{a^2}{b^2}\cos^2\theta\right)^{-1/2} \tag{5}$$

where θ is the polar angle, while a and b are the major and minor diameters, respectively. The spheroid aspect ratio is defined as $\epsilon = a/b$. Note that ϵ is always greater than 1.0 since a is the major diameter [34]. The equivalent diameter of the sphere having the same surface area as the spheroid is given by [34]

$$d_s = \frac{1}{2}\left(2a^2 + 2ab\frac{\sin^{-1}e}{e}\right)^{1/2} \quad \text{where } e = \frac{(\epsilon^2-1)^{1/2}}{\epsilon} \tag{6}$$

Moreover, the number frequency of equivalent diameter d_s denoted by $f(d_s)$ is defined as

$$f(d_s) = \frac{N(d_s)}{\int_o^\infty N(d_s)\,\mathrm{d}d_s} = \frac{N(d_s)}{N_T} \tag{7}$$

where $N(d_s)$ is the number of cells per unit volume of suspension having diameter between d_s and $d_s + \mathrm{d}d_s$. The denominator on the right-hand side of Eq. (7) is the total cell concentration N_T expressed in total number of cells per m^3 of suspension.

Berberoğlu et al. [3,9] reported the size distribution for the minor and major diameters $N(a)$ and $N(b)$ for each *C. reinhardtii* strain (see Fig. 2 in Ref. [3]). Their average circularity is defined as $c = 4\pi \times A_S/P^2$ where A_S and P are the cell's surface area and perimeter.[1] The authors used the image analysis software ImageJ [59] to measure their minor and major diameters assuming the cells to be 2D ellipses. Then, the surface area and perimeter of axisymmetric spheroids were calculated as $A_S = \pi ab/4$ and $P = 2\pi\sqrt{2(a^2+b^2)}$, respectively. The circularity of *C. reinhardtii* CC125, *tla1*, *tlaX*, and *tla1-CW$^+$* was 0.989, 0.996, 0.979, and 0.986, respectively while their average aspect ratio ϵ was 1.149, 1.073, 1.220, and 1.173, respectively. Similarly, the number frequencies for *B. braunii*, *Chlorella sp.*, and *C. littorale* were reported in Ref. [9]. Their circularity was equal to 0.961, 0.965, and 0.975 while their average aspect ratio ϵ was 1.333, 1.301, and 1.212, respectively.

Finally, Fig. 2 shows the number frequency $f(d_s)$ of the equivalent diameter d_s for *C. reinhardtii* CC125 and its truncated chlorophyll antenna transformants. It was calculated from experimentally measured major and minor diameters using Eq. (6). Similarly, Fig. 3 shows the number frequency $f(d_s)$ for *B. braunii*, *Chlorella sp.*, and *C. littorale*. Depending on the species, the number of bins was 60 or 70 with d_s ranging between 2 and 20 μm.

3.4. Prediction of the radiation characteristics of microalgae

The Lorentz–Mie theory predicts the absorption and scattering cross-sections denoted by $C_{abs,\lambda}(d_s)$ and $C_{sca,\lambda}(d_s)$ (expressed in m^2) of an individual spherical cell of diameter d_s with complex index of refraction $n_\lambda + ik_\lambda$ submerged in phosphate buffered saline (PBS) solution with refraction index n_{PBS}. Then, the absorption coefficient κ_λ of a microorganism suspension with size distribution

---

[1] Note that the circularity was mistakenly calculated as $4\pi \times (A_S/P)^2$ in Ref. [3] and $4\pi \times A_S/P$ in Ref. [9]. This did not have any consequence on the reported radiation characteristics used here.
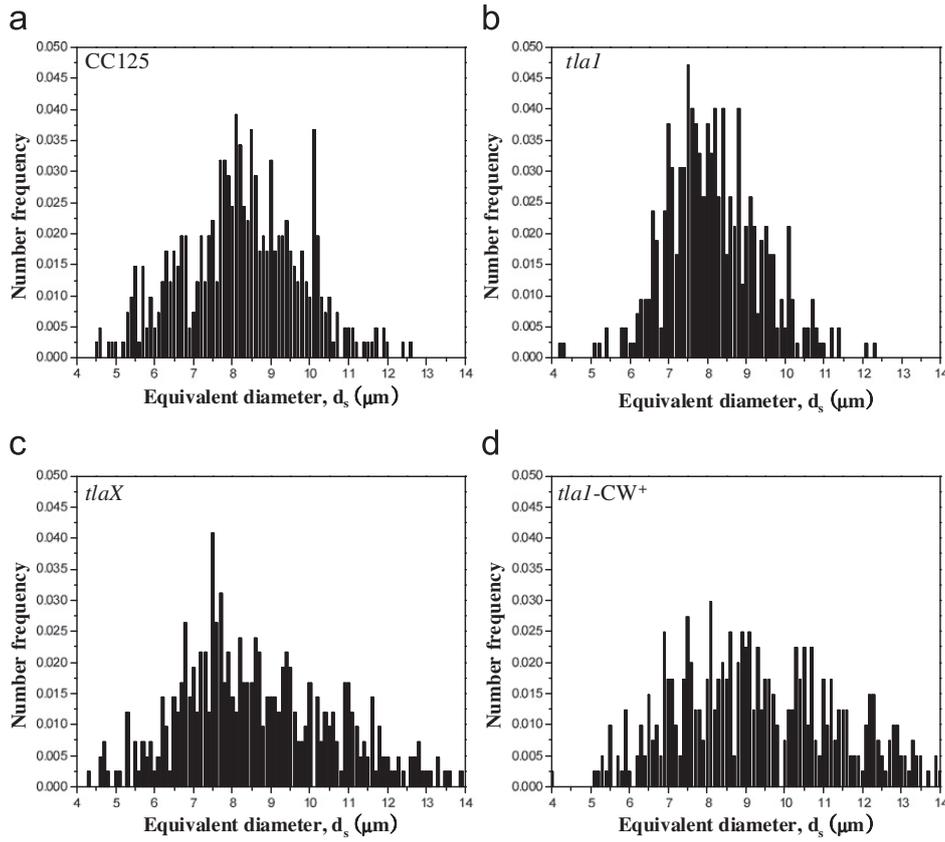
Fig. 2. Number frequency $f(d_s)$ of the equivalent sphere diameter of (a) *C. reinhardtii* CC 125 ($c=0.989$, $\epsilon=1.149$) and its truncated chlorophyll antenna transformants (b) *tla1* ($c=0.996$, $\epsilon=1.073$), (c) *tlaX* ($c=0.979$, $\epsilon=1.220$), and (d) *tla1-CW*$^+$ ($c=0.986$, $\epsilon=1.173$). The equivalent diameter was estimated from Eq. (6) and major and minor diameter distributions reported in Fig. 2 in Ref. [3].

$N(d_s)$ is expressed as [60]

$$\kappa_\lambda = \int_0^\infty C_{abs,\lambda}(d_s)N(d_s)\,\mathrm{d}d_s = \overline{C}_{abs,\lambda}N_T \qquad (8)$$

Similarly, the effective scattering coefficient of the microorganisms $\sigma_{s,\lambda}$ can be written as [61]

$$\sigma_{s,\lambda} = \int_0^\infty C_{sca,\lambda}(d_s)N(d_s)\,\mathrm{d}d_s = \overline{C}_{sca,\lambda}N_T \qquad (9)$$

Here, $\overline{C}_{abs,\lambda}$ and $\overline{C}_{sca,\lambda}$ are the average absorption and scattering cross-sections of the microalgae in suspension (in m^2), respectively. These average cross-sections can effectively be measured for typically polydisperse microalgae population. In fact, Berberoğlu et al. [9] measured the average absorption and scattering cross-sections $\overline{C}_{abs,\lambda}$ and $\overline{C}_{sca,\lambda}$ for *B. braunii*, *Chlorella sp.*, and *C. littorale*. Thus, the predictions from the Lorentz–Mie theory and Eqs. (8) and (9) could be directly compared with experimental data.

Berberoğlu et al. [3] measured the average mass absorption and scattering cross-sections of *C. reinhardtii* and its mutants denoted by $\overline{A}_{abs,\lambda}$ and $\overline{S}_{sca,\lambda}$, expressed in m^2/kg, and defined as

$$\overline{A}_{abs,\lambda} = \kappa_\lambda/X \quad \text{and} \quad \overline{S}_{sca,\lambda} = \sigma_{s,\lambda}/X \qquad (10)$$

where X is the microorganism concentration expressed in kilogram of dry cell weight per cubic meter of liquid medium. The average absorption and scattering cross-sections $\overline{C}_{abs,\lambda}$ and $\overline{C}_{sca,\lambda}$ can be calculated from the average mass absorption and scattering cross-sections

$\overline{A}_{abs,\lambda}$ and $\overline{S}_{sca,\lambda}$ according to [4]

$$\overline{C}_{abs,\lambda} = \overline{A}_{abs,\lambda}V_{32}\rho_{dm}(1-x_w) \quad \text{and}$$

$$\overline{C}_{sca,\lambda} = \overline{S}_{sca,\lambda}V_{32}\rho_{dm}(1-x_w) \qquad (11)$$

where the density of *C. reinhardtii* and its mutants ρ_{dm} was taken as 1350 kg/m^3 as reported in the literature [62]. Their mean particle volume V_{32} was computed from their respective Sauter mean diameter as 3.36×10^{-16} m^3 for CC125, 3.04×10^{-16} m^3 for *tla1*, 4.27×10^{-16} m^3 for *tlaX*, and 5.24×10^{-16} m^3 for *tla1-CW*$^+$. Note that Pottier et al. [4] used a similar value of $V_{32}=3.19 \times 10^{-16}$ m^3 for their *C. reinhardtii* strain. Finally, x_w was taken as 0.78 for *C. reinhardtii* and its mutants [4].

3.5. Optimization algorithm

Fig. 4 shows the schematic diagram of the procedure used to simultaneously retrieve the spectral refraction index n_λ and the absorption index k_λ. The Lorentz–Mie theory [7] was employed in the forward model to calculate the spectral average absorption and scattering cross-sections $\overline{C}_{abs,\lambda}$ and $\overline{C}_{sca,\lambda}$ over the PAR.

Various optimization algorithms can be used to efficiently and simultaneously determine n_λ and k_λ. The objective is to find the values of these parameters that minimize the difference between the predicted and experimentally measured absorption and scattering cross-sections of the microalgal suspension in the least-square sense.

a

b

c
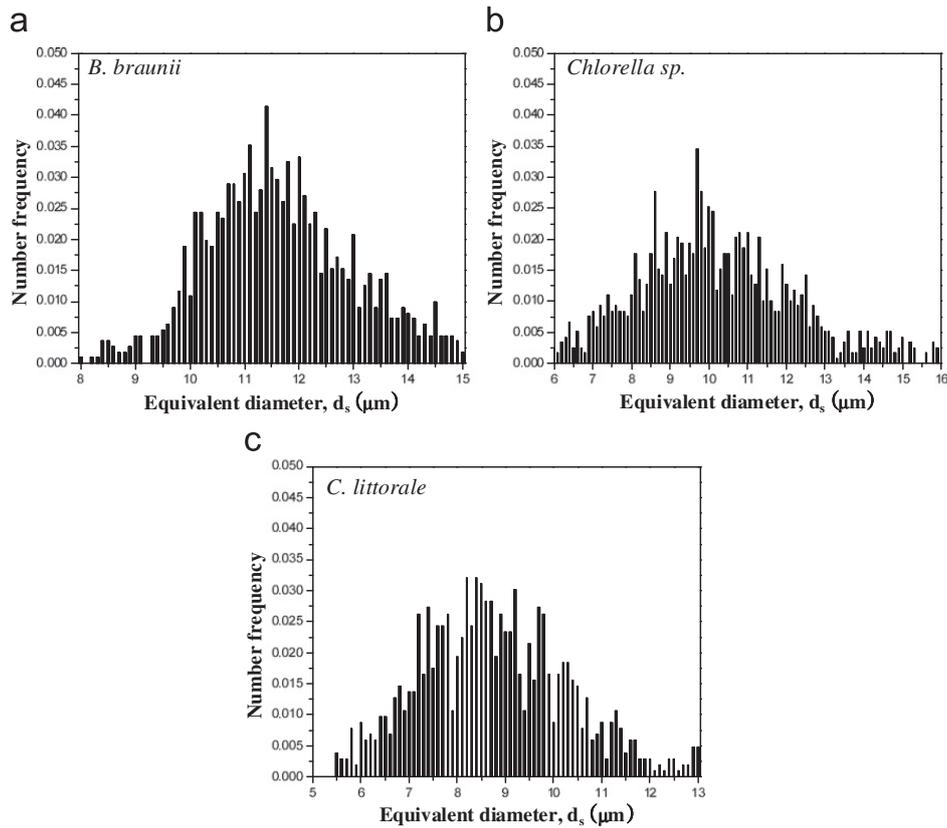
Fig. 3. Number frequency $f(d_s)$ of the equivalent sphere diameter of (a) *B. braunii* ($c=0.961$, $\epsilon=1.333$), (b) *Chlorella sp.* ($c=0.965$, $\epsilon=1.301$), and (c) *C. littorale* ($c=0.975$, $\epsilon=1.212$). The equivalent diameter was estimated from Eq. (6) and major and minor diameter distributions reported in Fig. 2 in Ref. [9].
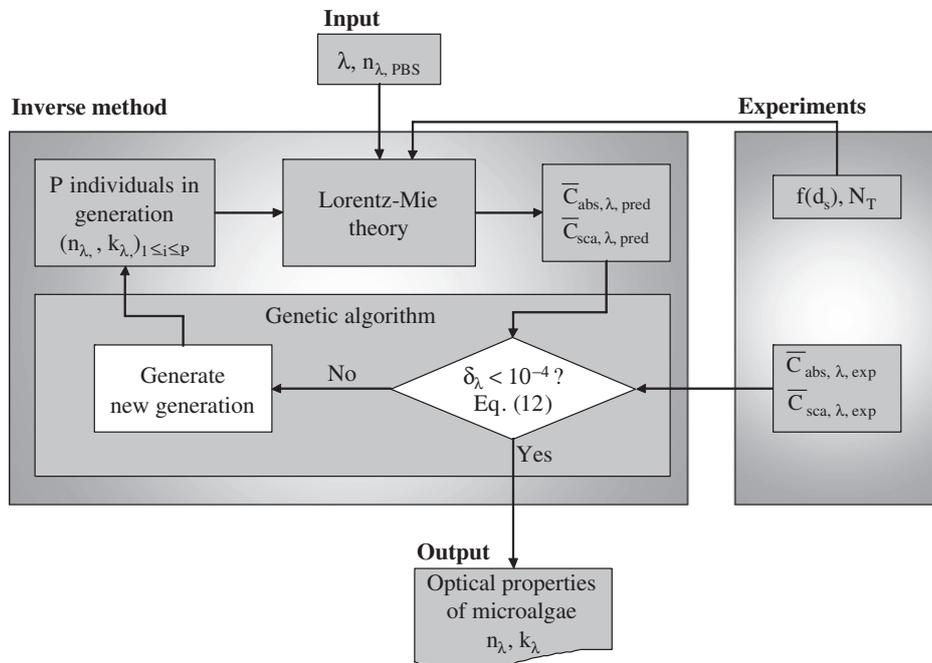
Fig. 4. Block diagram of the procedure used to retrieve the refraction index n_λ and absorption index k_λ from the absorption and scattering cross-sections $\overline{C}_{abs,\lambda}$ and $\overline{C}_{sca,\lambda}$ at a given wavelength λ for number frequency $f(d_s)$. We used $N=120$ individuals per generation for a maximum of 50 generations. n_λ and k_λ were allowed to range from 1.33 to 1.53 and from 10^{-5} to 0.01, respectively.

Genetic algorithm can find a global minimum of an objective function using the concept of evolution theory [63]. A given set of input parameters [e.g., (n_λ, k_λ)] is called an individual and each parameter is called a gene. The numerical procedure starts with a randomly generated population consisting of numerous individuals. The objective

function (or fitness function) is calculated for each individual of the population and estimates some difference between experimental measurements and model predictions. Individuals with the largest value of the objective function are dismissed. Those with the smallest objective function are selected to form a new population. Breeding of the new generation consists of producing new individuals by recombination and random mutation of the genes of an arbitrary pair of individuals. The fitness function is evaluated for each individual and the procedure is repeated generation after generation until the objective function falls below a given convergence criterion. This method tends to be slow but it is robust and eventually converges to the global minimum [64].

In the present study, genetic algorithm was implemented using the general purpose function optimization code PIKAIA [65–67]. Here, the spectral refraction index n_λ was assumed to range from 1.33 to 1.53 based on the literature [4,68]. On the other hand, the absorption index k_λ was allowed to range from 10^{-5} to 0.01. For each wavelength, the objective function δ_λ was defined as

$$\delta_\lambda = \left(\frac{\overline{C}_{abs,\lambda,pred} - \overline{C}_{abs,\lambda,exp}}{\overline{C}_{abs,\lambda,exp}}\right)^2 + \left(\frac{\overline{C}_{sca,\lambda,pred} - \overline{C}_{sca,\lambda,exp}}{\overline{C}_{sca,\lambda,exp}}\right)^2 \quad (12)$$

The genetic algorithm used a maximum of 50 generations with population of $P = 120$ individuals. The convergence criteria was set as $\delta_\lambda < 10^{-4}$.

3.6. Experimental uncertainties

Experimentally, the absorption and scattering cross-sections for each species were measured for three different microalgae concentrations. The maximum experimental uncertainties, with 95% interval confidence, associated with the absorption and scattering cross-sections were 6%, 8%, 16%, and 6% for *C. reinhardtii* CC125, *tla1*, *tlaX*, and *tla1-CW$^+$*, respectively. The maximum uncertainties associated with $\overline{C}_{abs,\lambda}$ and $\overline{C}_{sca,\lambda}$ for *B. braunii*, *Chlorella sp.*, and *C. littorale* were 21%, 15%, and 15%, respectively. These experimental uncertainties propagated in the retrieved values of n_λ and k_λ. Thus, to estimate the uncertainties for n_λ and k_λ they were retrieved at wavelengths 435 and 676 nm, corresponding to Chl *a* absorption peaks, from the cross-sections $\overline{C}_{abs,\lambda} \pm \Delta\overline{C}_{abs,\lambda}$ and $\overline{C}_{sca,\lambda} \pm \Delta\overline{C}_{sca,\lambda}$ where $\Delta\overline{C}_{abs,\lambda}$ and $\Delta\overline{C}_{sca,\lambda}$ were equal to two standard deviations.

4. Results and discussion

4.1. Validation: retrieving n_λ and d_s of monodisperse latex particles

Berberoğlu et al. [3] measured the scattering cross-section, between 400 and 800 nm, of monodisperse polystyrene latex spheres 5 μm in diameter in suspension in PBS solution. They used the same experimental procedure and analysis as that used to measure the radiation characteristics of the different microalgae considered in the present study. For validation purposes, the previously described inverse procedure and associated algorithm were used to retrieve the spectral refraction index as well

as the diameter of spherical polystyrene latex particles using the measured scattering cross-section [3].

First, the absorption index of PBS in the visible was reported to be that of water [69] which is less than 4.0×10^{-8} [70]. The absorption index of polystyrene was reported to be less than 5.0×10^{-3} [71] between 400 and 700 nm. Thus, in the present study, the absorption index of both polystyrene and PBS were taken as $k = 0.0$ used as input parameters in the Lorentz–Mie theory. On the other hand, the refraction index of both PBS and polystyrene were modeled by the Cauchy dispersion relation expressed as [72]

$$n_\lambda = A + \frac{B}{\lambda^2} + \frac{C}{\lambda^4} \quad (13)$$

For PBS, the parameters A_{PBS}, B_{PBS}, and C_{PBS} were taken as $A_{PBS} = 1.32711$, $B_{PBS} = 2.6 \times 10^{-3}$ μm^2, and $C_{PBS} = 5.0 \times 10^{-5}$ μm^4 when λ was expressed in μm [69]. Then, our inverse method simultaneously retrieved the particle diameter d_s and the parameters A, B, and C using the objective function

$$\delta_\lambda = \sum_{i=1}^{9} \left(\frac{\overline{C}_{sca,\lambda_i,pred} - \overline{C}_{sca,\lambda_i,exp}}{\overline{C}_{sca,\lambda_i,exp}}\right)^2 \quad (14)$$

where the nine wavelengths λ_i were uniformly distributed between 400 and 700 nm. The parameters were found to be respectively $d_s = 5.01$ μm, $A = 1.5555$, $B = 3.911 \times 10^{-3}$ μm^2, and $C = 3.867 \times 10^{-4}$ μm^4. First, the polystyrene sphere diameter was retrieved very accurately. The values of parameters A, B, and C should be compared with those reported by Ma et al. [71] as $A = 1.5725$, $B = 3.108 \times 10^{-3}$ μm^2, and $C = 3.4779 \times 10^{-4}$. Comparison (not shown) of the refraction index of polystyrene retrieved here and that reported by Ma et al. [71] indicated that the relative error was less than 1.2% for all wavelengths between 400 and 800 nm. This is in excellent agreement and confirms the validity of the methodology and the proper implementation of the genetic algorithm.

4.2. Retrieved spectral complex index of refraction of microalgae

4.2.1. C. reinhardtii CC125 and its truncated chlorophyll antenna transformants tla1, tlaX, and tla1-CW$^+$

This section presents the retrieved spectral complex index of refraction of *C. reinhardtii* CC125 and its truncated chlorophyll antenna transformants *tla1*, *tlaX*, and *tla1-CW$^+$*. The spectral complex index of refraction was retrieved at 36 different wavelengths uniformly distributed over the spectral region from 400 to 750 nm with 10 nm increments.
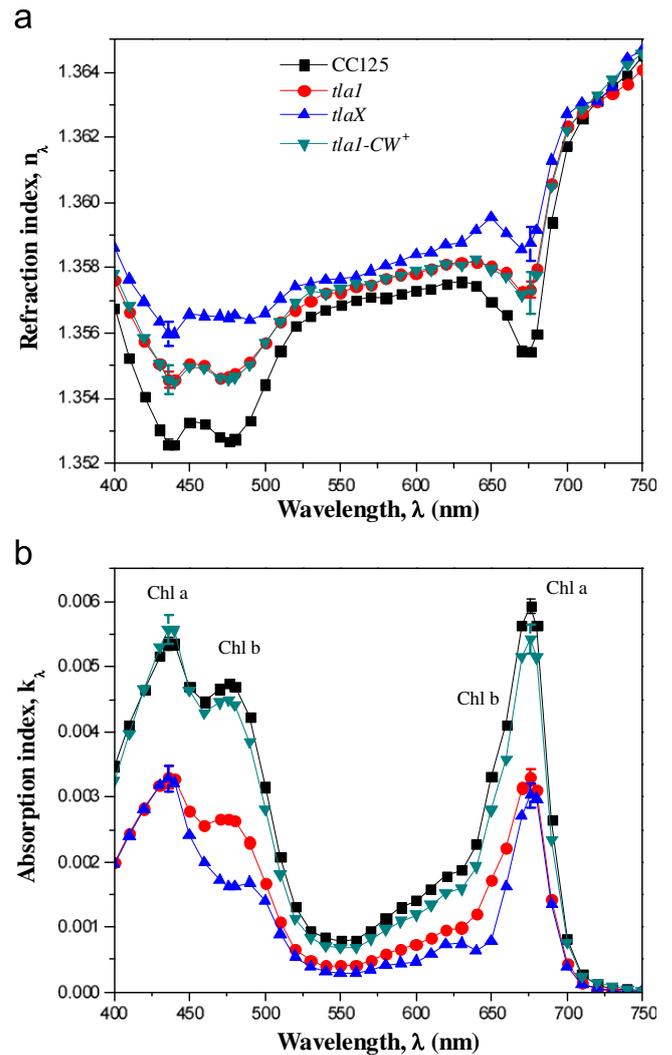
Fig. 5(a) and (b) shows the retrieved effective refraction and absorption indices of *C. reinhardtii* CC 125 between 400 and 750 nm, respectively. Here, the microalgae were assumed to be spherical with (i) the major diameter number frequency $f(a)$ and (ii) the minor diameter number frequency $f(b)$, or with (iii) the equivalent diameter number frequency $f(d_s)$ shown in Fig. 2. In all cases, the retrieved value of n_λ of *C. reinhardtii* CC 125 was

a

b
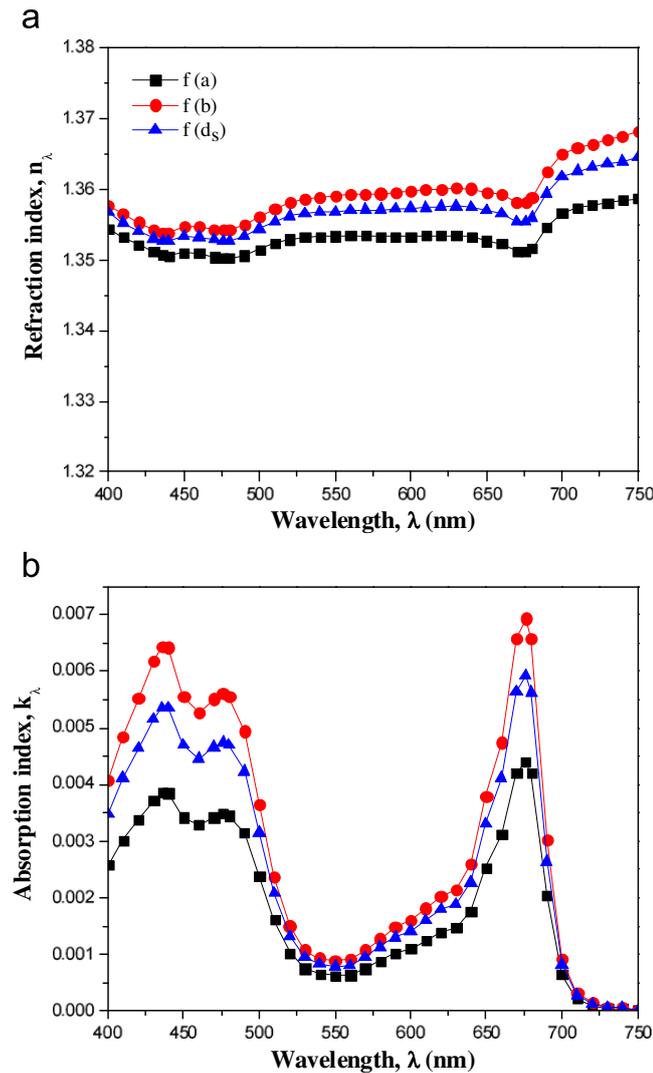
Fig. 5. Comparison of the retrieved refraction and absorption indices between 400 and 750 nm for the green algae *C. reinhardtii* CC 125 using major, minor, and equivalent diameter distributions $f(a)$, $f(b)$, and $f(d_s)$, respectively.

a

b

Fig. 6. Comparison of the retrieved refraction and absorption indices between 400 and 750 nm for the green algae *C. reinhardtii* CC 125 and its truncated chlorophyll antenna transformants *tla1*, *tlaX*, and *tla1-CW$^+$* using their number frequency $f(d_s)$ shown in Fig. 2.

slightly dependent on wavelength but significantly different from the constant value of 1.527 assumed by Pottier et al. [4]. Instead, the retrieved value of n_λ was around 1.36 which is similar to the refraction index of phytoplanktons reported in the literature [68]. Note that the effective refraction index retrieved by using the major and the minor diameter number frequencies differed from that obtained using the equivalent diameter distribution by less than 0.3% in the wavelength range considered. Moreover, the maximum relative differences between the retrieved absorption index k_λ using the equivalent diameter d_s and that using the major and the minor diameter distributions was 23%. In other words, the retrieved k_λ was more sensitive to the size distribution than n_λ. For both n_λ and k_λ, the values retrieved using $f(a)$ and $f(b)$ provided the upper and lower bounds for those retrieved using $f(d_s)$, respectively.

Fig. 6(a) and (b) respectively compares the effective refraction and absorption indices for *C. reinhardtii* CC 125 and its truncated chlorophyll antenna transformants *tla1*,

tlaX, and *tla1-CW$^+$* between 400 and 750 nm. Here, n_λ and k_λ were retrieved using the equivalent diameter distribution $N(d_s)$. Fig. 6(a) indicates that n_λ ranged between 1.350 and 1.365 between 400 and 750 nm. Overall, n_λ varied slightly from one strain to another. On the other hand, Fig. 6(b) clearly shows that the absorption index decreases from CC 125 to *tla1-CW$^+$*, *tla1*, and *tlaX* corresponding to a reduction in the size of their chlorophyll antenna. A significant decrease in k_λ was apparent for *tlaX* at wavelength 475 nm corresponding to a decrease in Chl *b* concentration caused by genetic engineering. In addition, *tla1-CW$^+$* features an absorption index larger than *tla1* possibly due to the presence of a cell wall [49]. It is also interesting to note that (i) the retrieved n_λ and k_λ were continuous functions of wavelength and that (ii) the absorption peaks of *in vivo* Chl *a* at 435 and 676 nm and Chl *b* at 475 and 650 nm were distinctly apparent. This further provides confidence in the inverse method and the results since both n_λ and k_λ were retrieved for each wavelength independently.

Finally, Fig. 7 compares the spectral absorption and scattering cross-sections measured experimentally and those predicted by Eq. (8) using the Lorentz–Mie theory and the retrieved value of the optical properties of each *C. reinhardtii* strains between 400 and 750 nm. It shows excellent agreement at all wavelengths. The average relative and maximum errors between experimental measurements and the predictions between 400 and 700 nm were respectively (i) less than 0.3% and 1.4% for the average absorption cross-section $\overline{C}_{abs,\lambda}$ and (ii) less than 0.2% and 0.8% for the average scattering cross-section $\overline{C}_{sca,\lambda}$ for all strains.

4.2.2. B. braunii, Chlorella sp., and C. littorale

This section presents the retrieved effective refraction and absorption indices of *B. braunii*, *Chlorella sp.*, and *C. littorale* between 400 and 750 nm. The same procedure and ranges of n_λ and k_λ as those previously implemented
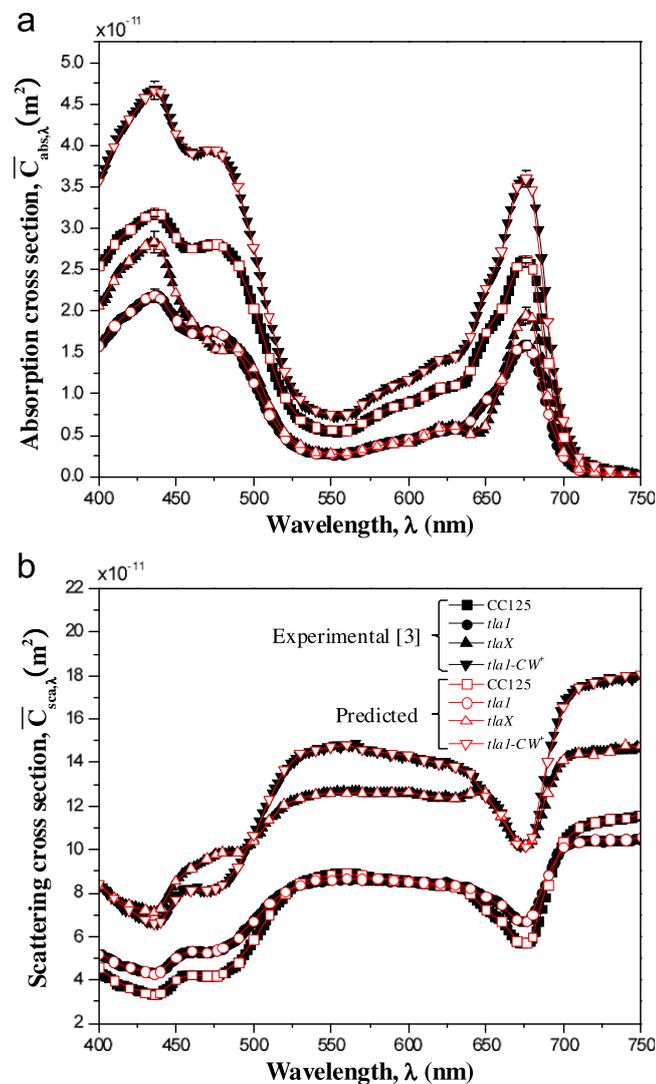
for *C. reinhardtii* were used based on the measured average absorption and scattering cross-sections $\overline{C}_{abs,\lambda}$ and $\overline{C}_{sca,\lambda}$ [9].

Fig. 8(a) shows the retrieved effective refraction and absorption indices for *B. braunii*, *Chlorella sp.*, and *C. littorale* between 400 and 750 nm from the measured absorption and scattering cross-sections. Their refraction index n_λ varied slightly between 1.345 and 1.36. Fig. 8(a) indicates that *C. littorale* had the largest refraction index followed by *B. braunii* and *Chlorella sp.* This can be attributed to differences in their composition and in particular their carbohydrates and proteins content. Indeed, Aas [73] derived the refraction index of a phytoplankton cells from their metabolite composition by treating them as a "mixture" of various constituents. The author reported the refraction index of the major cell constituents including carbohydrates and proteins which have the largest refraction index in the PAR equal to 1.55 and 1.53, respectively. In addition, the dry mass fractions of carbohydrates and proteins were reported to be (a) 25% and 53% for *C. littorale* [20], (b) 17% and 32% for

Fig. 7. Comparison of the predicted and experimentally measured [3] average spectral absorption $\overline{C}_{abs,\lambda}$ and scattering $\overline{C}_{sca,\lambda}$ cross-sections of the green algae *C. reinhardtii* CC 125 and its truncated chlorophyll antenna transformants *tla1*, *tlaX*, and *tla1-CW$^+$*. Experimental data [9] for $\overline{A}_{abs,\lambda}$ and $\overline{S}_{sca,\lambda}$ were converted to $\overline{C}_{abs,\lambda}$ and $\overline{C}_{sca,\lambda}$ using Eqs. (10) and (11), respectively.
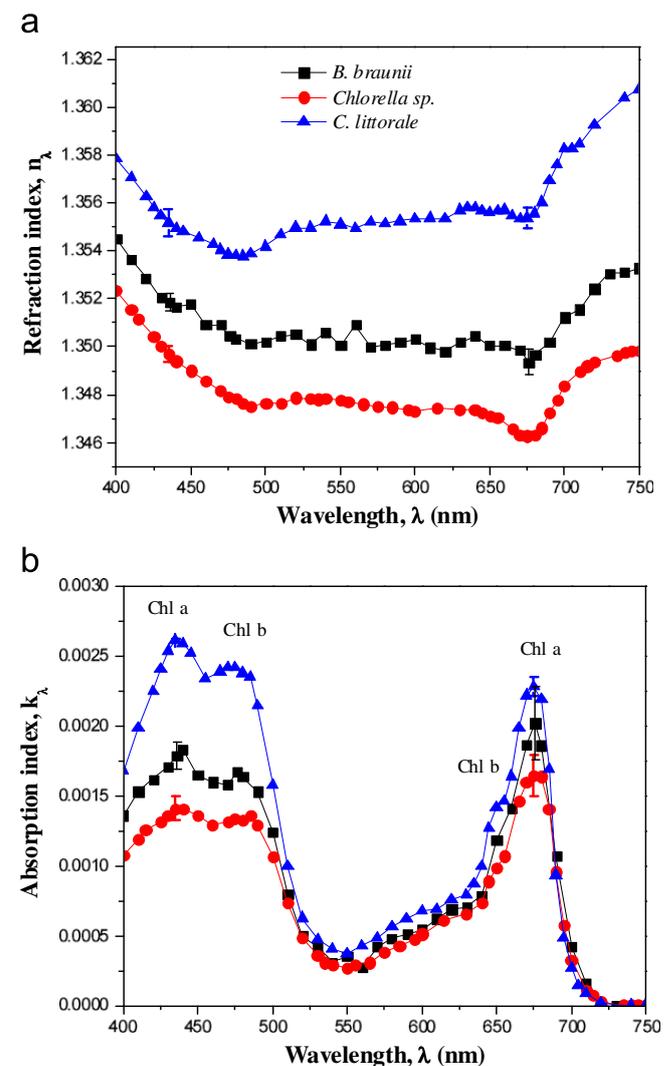
Fig. 8. Comparison of the retrieved refraction and absorption indices between 400 and 750 nm for *B. braunii*, *Chlorella sp.*, and *C. littorale* using their number frequency $f(d_s)$ shown in Fig. 3.

B. braunii [74], and (c) 19% and 6% for *Chlorella sp.* [19]. Assuming that the water volume fraction was similar for all three species, *C. littorale* feature the largest concentrations of carbohydrates and proteins followed by *B. braunii* and lastly *Chlorella sp.* The differences in these reported carbohydrates and proteins mass fractions could explain the differences observed in the retrieved refraction indices of these species.

Fig. 8(b) indicates that *C. littorale* had the largest absorption index k_λ while *B. braunii* and *Chlorella sp.* featured similar absorption indices across the PAR. Here also, k_λ features absorption peaks at 435, 475, and 676 nm corresponding to the absorption peaks of *in vivo* Chl *a* and Chl *b*. It is interesting to note that the absorption cross-section of *B. braunii* was larger than those of *C. littorale* and *Chlorella sp.* which were similar [9] despite the fact that *C. littorale* cells were much smaller than *B. braunii*, and *Chlorella sp.* However, the dry mass fraction of Chl $a+b$ was (a) 1.9% in *C. littorale* [20], (b) 0.22–0.56% in *B. braunii* [18], and (c) 0.4–1.41% in *Chlorella sp.* [19]. This may explain why *C. littorale* had the largest absorption index k_λ and *B. braunii* and *Chlorella sp.* were found to have similar k_λ.

Finally, the average relative and maximum errors between experimental measurements and the Lorentz–Mie theory predictions using the reported values for n_λ and k_λ were respectively (i) 0.4% and 3% for the absorption cross-sections and (ii) less than 0.5% and 2% for the scattering cross-sections of *B. braunii*, *Chlorella sp.*, and *C. littorale* between 400 and 750 nm.

4.3. Discussion

4.3.1. Retrieved optical properties

Figs. 6(a) and 8(a) indicate that the refraction index n_λ of all microorganisms features a small dip around 676 nm corresponding to a peak in k_λ caused by Chl *a* absorption. Such a dip was also observed around the same wavelength for various phytoplankton species as illustrated in Figs. 6.14 and 6.20 in Ref. [5]. This can be attributed to oscillator resonance around 676 nm. It can also be predicted by optical constant theory such as the Lorentz model [29] or the Helmholtz–Kettler theory [5]. Figs. 6 and 8 also show the error bars associated with the retrieved values of n_λ and k_λ resulting from the error propagation of uncertainties in the measured $\overline{C}_{abs,\lambda}$ and $\overline{C}_{sca,\lambda}$. The relative error corresponding to 95% confidence interval, associated with n_λ and k_λ was less than 0.1% and 7%, respectively for all the species considered. The absorption index was more sensitive to the experimental uncertainties than the refraction index. Nevertheless, the error propagation from the experimental measurements of $\overline{C}_{abs,\lambda}$ and $\overline{C}_{sca,\lambda}$ to the retrieved complex index of refraction was acceptable.

It is also important to note that the good agreement between measured and predicted cross-sections $\overline{C}_{abs,\lambda}$ and $\overline{C}_{sca,\lambda}$ reported for all species (e.g., Fig. 7) considered could not be obtained when (i) the refraction index n_λ of the microalgae was assumed to be constant over the PAR and (ii) k_λ was retrieved by optimizing the pigment mass fractions w_i for Chl *a*, Chl *b*, and PPC in Eq. (2). In other words, despite the fact that n_λ varies slightly over the PAR, it should not be treated as constant in predicting the microalgae absorption and scattering cross-sections.

4.3.2. Retrieved pigment concentrations of microalgae

The mass fractions of the three pigments Chl *a*, Chl *b*, and photoprotective carotenoids (PPC), denoted by w_a, w_b, and w_{PPC}, were estimated simultaneously from the retrieved absorption index k_λ for all species considered. The inverse method was also based on genetic algorithm and PIKAIA to minimize the objective function defined as

$$\Delta_\lambda = \sum_{i=1}^{36} \left(\frac{k_{\lambda_i,pred} - k_{\lambda_i}}{k_{\lambda_i}} \right)^2 \tag{15}$$

where $k_{\lambda_i,pred}$ is the absorption index predicted by Eq. (4) as a function of w_a, w_b, and w_{PPC}. Note that this approach relies on the validity of Eq. (4) and the database of *in vivo* spectral mass absorption coefficient Ea of various pigments reported in Ref. [12] and shown in Fig. 1.

Fig. 9 compares the absorption index previously retrieved and that predicted by Eq. (4) for *C. reinhardtii* CC 125 based on the fitted values $w_a = 16.50$ g/kg, $w_b = 9.68$ g/kg, and $w_{PPC} = 1.98$ g/kg. These values are in the same range as those measured by Pottier et al. [4] as $w_a = 14.00$ g/kg, $w_b = 7.00$ g/kg, $w_{PPC} = 4.50$ g/kg. It also shows the same comparison for *C. littorale* with the fitted values $w_a = 6.83$ g/kg, $w_b = 4.86$ g/kg, and $w_{PPC} = 1.32$ g/kg. It indicates that the previously retrieved k_λ and that predicted using the fitted pigment mass fractions were in fair agreement despite the inverse method used to minimize their difference. For example, the relative error between $k_{\lambda,pred}$ and k_λ for *C. reinhardtii* CC 125 at the absorption peaks of Chl *a* at 435 and 676 nm was 43% and 16%, respectively. For *C. littorale*, these relative errors were 36% and 25% at 435 and 676 nm, respectively. Similar results were obtained for the other strains of *C. reinhardtii* as well as for *B. braunii* and *Chlorella sp.*
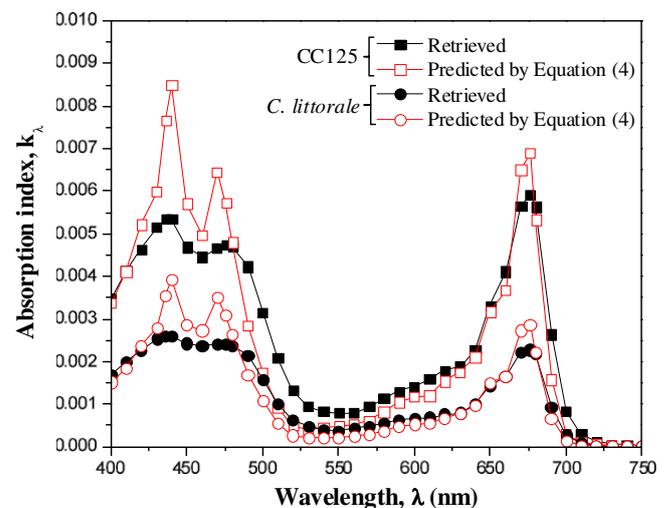

Fig. 9. Comparison between the retrieved absorption index k_λ and those predicted by Eq. (4) for (i) *C. reinhardtii* with $w_a = 16.50$ g/kg, $w_b = 9.68$ g/kg, and $w_{PPC} = 1.98$ g/kg and (ii) *C. littorale* with $w_a = 6.83$ g/kg, $w_b = 4.86$ g/kg, and $w_{PPC} = 1.32$ g/kg.

It is important to mention that Eqs. (1) and (4) are valid for a hypothetical slab of homogeneous and non-scattering microalgae materials for which the absorption coefficient is given by $\kappa_\lambda = 4\pi k_\lambda / \lambda$. The present results suggest that these equations apply only approximately to heterogeneous and spherical or spheroidal microalgae.

4.3.3. Compatibility with T-Matrix method

The above analysis and results rely on the assumptions that the different microalgae can be treated as spherical. However, their circularity and aspect ratio were not exactly unity [3,9]. To assess the validity and consequences of this assumption, the average absorption and scattering cross-sections $\overline{C}_{abs,\lambda}$ and $\overline{C}_{sca,\lambda}$ for *C. reinhardtii* CC 125 and *B. braunii* measured experimentally were compared with those predicted by the T-matrix method using the retrieved values of n_λ and k_λ. *B. braunii* was of particular interest because it featured the largest average aspect ratio of 1.333 and thus, was the most likely species to show large differences between experimental measurements and predictions by the T-matrix method. The predictions used (i) the average aspect ratio $\epsilon = 1.149$ for *C. reinhardtii* CC 125 and $\epsilon = 1.333$ for *B. braunii*, (ii) their equivalent diameter distribution $f(d_s)$ shown in Figs. 2 and 3, and (iii) their refraction and absorption indices retrieved using the Lorentz–Mie theory shown in Figs. 6 and 8, respectively. The results show that accounting for the non-sphericity of microalgae via the T-matrix method had relatively small effect on both $\overline{C}_{abs,\lambda}$ and $\overline{C}_{sca,\lambda}$ for both species. In fact, the maximum relative difference between T-matrix predictions and experimental data for both $\overline{C}_{abs,\lambda}$ and $\overline{C}_{sca,\lambda}$ was 1.8% for *C. reinhardtii* and 3.9% for *B. braunii*. Similar or better results were obtained for the other species since their average aspect ratio was closer to unity when the Lorentz–Mie theory is valid.

Overall, the effective refraction and absorption indices n_λ and k_λ retrieved over the PAR for all species considered in the present study can be used in the Lorentz–Mie theory along with their size distribution to accurately predict their radiation characteristics.

5. Conclusion

This paper presented and used a methodology to retrieve the spectral refraction and absorption indices of various biofuel producing microalgae from experimentally measured average absorption and scattering cross-sections between 400 and 750 nm. The microalgae were treated as spherical particles with equivalent diameter distributions calculated from experimentally measured major and minor diameter distributions. An inverse method was developed combining Lorentz–Mie theory as the forward method and genetic algorithm. The retrieved refraction and absorption indices were continuous functions of wavelength with apparent absorption peaks corresponding to those of *in vivo* Chl *a* and *b*. These optical properties can be used to predict the radiation characteristics of the species considered using Lorentz–Mie theory for a given size distribution.

Finally, the retrieved values of n_λ and k_λ between 400 and 750 nm for all microalgae considered in this study and shown in Figs. 6 and 8 are available in digital form online [75] or directly from the corresponding author upon request.

References

[1] Pilon L, Berberoğlu H, Kandilian R. Radiation transfer in photo-biological carbon dioxide fixation and fuel production by microalgae. J Quant Spectrosc Radiat Transfer 2011;112(17): 2639–60.

[2] Berberoğlu H, Pilon L. Experimental measurement of the radiation characteristics of *Anabaena variabilis* ATCC 29413-U and *Rhodobacter sphaeroides* ATCC 49419. Int J Hydrogen Energy 2007;32(18): 4772–85.

[3] Berberoğlu H, Melis A, Pilon L. Radiation characteristics of *Chlamydomonas reinhardtii* CC125 and its truncated chlorophyll antenna transformants *tla1*, *tlaX*, and *tla1-CW$^+$*. Int J Hydrogen Energy 2008;33(22):6467–83.

[4] Pottier L, Pruvost J, Deremetz J, Cornet JF, Legrand J, Dussap CG. A fully predictive model for one-dimensional light attenuation by *Chlamydomonas reinhardtii* in a torous photobioreactor. Biotechnol Bioengin 2005;91:569–82.

[5] Jonasz M, Fournier GR. Light scattering by particles in water: theoretical and experimental foundations San Diego, CA: Academic Press; 2007.

[6] Bricaud A, Morel A. Light attenuation and scattering by phytoplanktonic cells: a theoretical modelingAppl Opt 1986;25: 571–80.

[7] Mie G. Beiträge zur Optik trüber Medien, speziell kolloidaler Metallösungen. Ann Phys 1908;25(3):377–445.

[8] Mishchenko MI, Travis LD. Capabilities and limitations of a current FORTRAN implementation of the T-matrix method for randomly oriented, rotationally symmetric scatterers. J Quant Spectrosc Radiat Transfer 1998;60(3):309–24.

[9] Berberoğlu H, Gomez PS, Pilon L. Radiation characteristics of *Botryococcus braunii*, *Chlorococcum littorale*, and *Chlorella sp.* used for CO$_2$ fixation and biofuel production. J Quant Spectrosc Radiat Transfer 2009;110:1879–93.

[10] Ke B. Photosynthesis, photobiochemistry and photobiophysics. Dordrecht, The Netherlands: Kluwer Academic Publishers; 2001.

[11] Harris EH. The chlamydomonas sourcebook, vol. 1. San Diego, CA: Academic Press; 1989.

[12] Bidigare R, Ondrusek M, Morrow J, Kiefer D. In vivo absorption properties of algal pigments. Ocean Opt X 1990;1302:290–301.

[13] Wang LJ, Weller CL. Recent advances in extraction of nutraceuticals from plants. Trends Food Sci Technol 2006;17(6):300–12.

[14] Hosikian A, Lim S, Halim R, Danquah MK. Chlorophyll extraction from microalgae: a review on the process engineering aspects. Int J Chem Eng 2010;2010:11.

[15] Porra RJ, Thompson WA, Kriedemann PE. Determination of accurate extinction coefficients and simultaneous equations for assaying chlorophylls a and b extracted with four different solvents: verification of the concentration of chlorophyll standards by atomic absorption spectroscopyBiochim Biophys Acta (BBA): Bioenerget 1989;975(3):384–94.

[16] Ritchie R. Consistent sets of spectrophotometric chlorophyll equations for acetone, methanol and ethanol solvents. Photosynth Res 2006;89:27–41.

[17] Belcher JH. Notes on the physiology of *Botryococcus braunii* Kiitzing. Arch Microbiol 1968;61(4):335–46.

[18] Tanoi T, Kawachi M, Watanabe MM. Effects of carbon source on growth and morphology of *Botryococcus braunii*. J Appl Phycol 2011;23(1):25–33.

[19] Brown MR, Jeffrey SW. Biochemical composition of microalgae from the green algal classes Chlorophyceae and Prasinophyceae.

1. Amino acids, sugars and pigments. J Exp Mar Biol Ecol 1992; 161(1):91–113.

[20] Hu Q, Kurano K, Kawachi M, Iwasaki I, Miyachi S. Ultrahigh cell density culture of a marine green algae *Chlorococcum littorale* in a flat plate photobioreactor. Appl Microbiol Biotechnol 1998;49: 655–62.

[21] Schnackenberg J, Ikemoto H, Miyachi S. Relationship between oxygen-evolution and hydrogen-evolution in a *Chlorococcum* strain with high CO₂-tolerance. J Photochem Photobiol B: Biol 1995;28(2):171–4.

[22] Daniel KJ, Laurendeau NM, Incropera FP. Prediction of radiation absorption and scattering in turbid water bodies. ASME J Heat Transfer 1979;101:63–7.

[23] Agrawal BM, Mengüç MP. Forward and inverse analysis of single and multiple scattering of collimated radiation in an axisymmetric system. Int J Heat Mass Transfer 1991;34:633–47.

[24] Stramski D, Mobley CD. Effect of microbial particles on oceanic optics: a database of single-particle optical properties. Limnol Oceanogr 1997;42:538–49.

[25] Bidigare RR, Smith RC, Baker KS, Marra J. Oceanic primary production estimates from measurements of spectral irradiance and pigment concentrations. Global Biogeochem Cycles 1987;1: 171–86.

[26] Quirantes A, Bernard S. Light scattering by marine algae: two-layer spherical and nonspherical models. J Quant Spectrosc Radiat Transfer 2004;89(1–4):311–21.

[27] Bernard S, Probyn TA, Barlow RG. Measured and modelled optical properties of particulate matter in the southern benguela. South Afr J Sci 2001;97:410–20.

[28] Stramski D, Bricaud A, Morel A. Modeling the inherent optical properties of the ocean based on the detailed composition of planktonic community. Appl Opt 2001;40:2929–45.

[29] Bohren CF, Huffman DR. Absorption and scattering of light by small particles. New York, NY: John Wiley & Sons; 1998.

[30] Van De Hulst HC. Light scattering by small particles. New York, NY: Wiley; 1957.

[31] Bricaud A, Ronald J, Zaneveld V, Kitchen JC. Backscattering efficiency of coccolithophorids: use of a three-layered sphere model. Proc SPIE 1992;1750:27–33.

[32] Ronald J, Zaneveld V, Kitchen JC. The variation in the inherent optical properties of phytoplankton near an absorption peak as determined by various models of cell structure. Proc SPIE 1995;100:13309–20.

[33] Mishchenko MI, Hovenier JW, Travis LD. Light scattering by non-spherical particles. San Diego, CA: Academic Press; 2000.

[34] Mishchenko MI, Travis LD. Light scattering by polydispersions of randomly oriented spheroids with sizes comparable to wavelengths to observation. Appl Opt 1994;33(30):7206–25.

[35] Bricaud A, Bédhomme AL, Morel A. Optical properties of diverse phytoplanktonic species: experimental results and theoretical interpretation. J Plankton Res 1988;10:851–73.

[36] Morel A, Ahn YH. Optics of heterotrophic nanoflagellates and ciliates: a tentative assessment of their scattering role in oceanic waters compared to those of bacterial and algal cells. J Mar Res 1991;49:177–202.

[37] Stramski D, Morel A, Bricaud A. Modeling the light attenuation and scattering by spherical phytoplanktonic cells: a retrieval of the bulk refractive index. Appl Opt 1988;27:3954–7.

[38] Bryant FD, Seiber BA, Latimer P. Absolute optical cross sections of cells and chloroplasts. Arch Biochem Biophys 1969;135:79–108.

[39] Green RE, Sosik HM, Olson RJ, Durand MD. Flow cytometric determination of size and complex refractive index for marine particles: comparison with independent and bulk estimates. Appl Opt 2003;42:526–41.

[40] Spinrad RW, Brown JF. Relative real refractive index of marine microorganisms: a technique for flow cytometric estimation. Appl Opt 1986;25:1930–4.

[41] Gerhardt P, Beaman TC, Corner TR, Greenamyre JT, Tisa LS. Photometric immersion refractometry of bacterial spores. J Bacteriol 1982;150:643–8.

[42] Jonasz M, Fournier G, Stramski D. Photometric immersion refractometry: a method for determining the refractive index of marine microbial particles from beam attenuation. Appl Opt 1997;36(18): 4214–25.

[43] Barer R, Joseph S. Refractometry of living cells. Part I: basic principles. Quart J Microsc Sci 1954;96:399–423.

[44] DuRand MD, Olson RJ. Diel patterns in optical properties of the chlorophyte *Nannochloris sp.*: relating individual-cell to bulk measurements. Limnol Oceanogr 1998;43:1107–18.

[45] Cornet JF, Dussap CG, Dubertret G. A structured model for simulation of cultures of the cyanobacterium spirulina platensis in photobioreactors: I. Coupling between light transfer and growth kinetics. Biotechnol Bioengin 1992;40(7):817–25.

[46] Cornet JF, Dussap CG, Gross JB, Binois C, Lasseur C. A simplified monodimensional approach for modeling coupling between radiant light transfer and growth kinetics in photobioreactors. Chem Eng Sci 1995;50(9):1489–500.

[47] Duysens LM. The flattening of the absorption spectra of suspensions as compared to that of solutions. Biochim Biophys Acta 1956;19:1–12.

[48] Melis A, Zhang L, Forestier M, Ghirardi ML, Seibert M. Sustained photobiological hydrogen gas production upon reversible inactivation of oxygen evolution in the green alga *Chlamydomonas reinhardtii*. Plant Physiol 2000;117(1):129–39.

[49] Polle JE, Kanakagiri SD, Melis A. tlal, a DNA insertional transformant of the green alga *Chlamydomonas reinhardtii* with a truncated light-harvesting chlorophyll antenna size. Planta 2003;217(1): 49–59.

[50] Metzger P, Berkaloof C, Casadevall E, Coute A. Alkadiene- and botryococcene-producing races of wild strains of *Botryococcus braunii*. Phytochemistry 1985;24(10):2305–20.

[51] Sawayama S, Inoue S, Yokoyama S. Continuous culture of hydrocarbon-rich microalga *Botryococcus braunii* in secondarily treated sewage. Appl Microbiol Biotechnol 1994;41(6):729–31.

[52] Sheehan J, Dunahay T, Benemann J, Roessler P. A look back at the US Department of Energy's aquatic species program: biodiesel from algae. Technical report TP-580-24190, NREL; 1998.

[53] Chisti Y. Biodiesel from algae. Biotechnol Adv 2007;25:294–306.

[54] Lee JY, Kwon TS, Baek K, Yang JW. Biological fixation of CO₂ by *Chlorella sp.* HA-1 in a semi-continuous and series reactor system. J Microbiol Biotechnol 2005;15(3):461–5.

[55] Chiu SY, Kao CY, Chen CH, Kuan TC, Ong SC, Lin CS. Reduction of CO₂ by a high-density culture of *Chlorella sp.* in a semi-continuous photobioreactor. Bioresour Technol 2008;99(9): 3389–96.

[56] Kodama M, Ikemoto H, Miyachi S. A new species of highly CO₂-tolerant fast growing marine microalga suitable for high density culture. J Mar Biotechnol 1993;1:21–5.

[57] Quirantes A, Bernard S. Light-scattering methods for modelling algal particles as a collection of coated and/or nonspherical scatterers. J Quant Spectrosc Radiat Transfer 2006;100: 315–24.

[58] Baird ME. Numerical approximations of the mean absorption cross-section of a variety of randomly oriented microalgal shapes. J Math Biol 2003;47:325–36.

[59] Rasband WS. ImageJ, U.S. National Institute of Health, Bethesda, MD, USA; 1997–2007 ⟨http://rsb.info.nih.gov/ij/⟩.

[60] Modest MF. Radiative heat transfer. San Diego, CA: Academic Press; 2003.

[61] Berberoğlu H, Yin J, Pilon L. Simulating light transfer in a bubble sparged photobioreactor for simultaneous hydrogen fuel production and CO₂ mitigation. Int J Hydrogen Energy 2007;32(13): 2273–85.

[62] Eroglu E, Melis A. "Density equilibrium" method for the quantitative and rapid in situ determination of lipid, hydrocarbon, or biopolymer content in microorganisms. Biotechnol Bioeng 2009;102(5):1406–15.

[63] Baeck T. Genetic algorithms in theory and practice. Oxford, UK: The Oxford University Press; 1996.

[64] Charbonneau P. Genetic algorithms in astronomy and astrophysics. Astrophys J 1995;101:309.

[65] Charbonneau P, Knapp B. A User's guide to PIKAIA 1.0, Technical report. NCAR technical note 418+IA, National Center for Atmospheric Research; 1995.

[66] Charbonneau P. An introduction to genetic algorithms for numerical optimization. Technical report. NCAR Technical note 450+IA, National Center for Atmospheric Research; 2002.

[67] Charbonneau P. Release notes for PIKAIA 1.2. Technical report. NCAR technical note 451+STR, National Center for Atmospheric Research; 2002.

[68] Morel A, Bricaud A. Inherent optical properties of algal cells including picoplankton: theoretical and experimental results. Can Bull Fisher Aquat Sci 1986:521–60.

[69] Zhernovaya O, Sydoruk O, Tuchin V, Douplik A. The refractive index of human hemoglobin in the visible range. Phys Med Biol 2011;56(13):4013–21.

[70] Hale GM, Querry MR. Optical constants of water in the 200-nm to 200-m wavelength region. Appl Opt 1973;12:555563.

[71] Ma X, Lu JQ, Brock RS, Jacobs KM, Yang P, Hu HH. Determination of complex refractive index of polystyrene microspheres from 370 to 1610 nm. Phys Med Biol 2003;48:4165–72.

[72] Nikolov ID, Ivanov CD. Optical plastic refractive measurements in the visible and the near-infrared regions. Appl Opt 2000;39(13):2067–70.

[73] Aas E. Refractive index of phytoplankton derived from its metabolite composition. J Plankton Res 1996;18(12):2223–49.

[74] Ashokkumar V, Rengasamy R. Mass culture of *Botryococcus braunii* kutz. under open raceway pond for biofuel production. Bioresour Technol 2012;104:394–9.

[75] Pilon L. Optical constants of microalgae for biofuel production between 400 and 750 nm; 2012 ⟨http://www.seas.ucla.edu/~pilon/downloads.htm⟩ and ⟨http://repositories.cdlib.org/escholarship/⟩.